Chinese Journal of Oceanology and Limnology
Vol. 30 No. 2, P. 295-304, 2012
DOI: http://dx.doi.org/10.1007/s00343-012-1094-y

Assessment of total suspended sediment concentrations in Poyang Lake using HJ-1A/1B CCD imagery*

YU Zhifeng (于之锋)[1, 2, 4], CHEN Xiaoling (陈晓玲)[1, 3, **], ZHOU Bin (周斌)[2, 4], TIAN Liqiao (田礼乔)[1, **], YUAN Xiaohong (袁小红)[2, 4], FENG Lian (冯炼)[1]

[1] *State Key Laboratory of Information Engineering in Surveying, Mapping and Remote Sensing (LIESMARS), Wuhan University, Wuhan 430079, China*

[2] *Institute of Remote Sensing and Earth Sciences, Hangzhou Normal University, Hangzhou 311121, China*

[3] *Key Laboratory of Poyang Lake Wetland and Watershed Research, Ministry of Education, Jiangxi Normal University, Nanchang 330022, China*

[4] *Zhejiang Provincial Key Laboratory of Urban Wetlands and Regional Change, Hangzhou 311121, China*

Received Apr. 3, 2011; accepted in principle Apr. 27, 2011; accepted for publication Jul. 26, 2011

Abstract We explored the potential of the environment and disaster monitoring and forecasting small satellite constellations (HJ-1A/1B satellites) charge-coupled device (CCD) imagery (spatial resolution of 30 m, revisit time of 2 days) in the monitoring of total suspended sediment (TSS) concentrations in dynamic water bodies using Poyang Lake, the largest freshwater lake in China, as an example. Field surveys conducted during October 17–26, 2009 showed a wide range of TSS concentration (3–524 mg/L). Atmospheric correction was implemented using the Fast Line-of-sight Atmospheric Analysis of Spectral Hypercubes (FLAASH) module in ENVI with the aid of aerosol information retrieved from concurrent Terra/Moderate Resolution Imaging Spectroradiometer (MODIS) surveys, which worked well at the CCD bands with relatively high reflectance. A practical exponential retrieval algorithm was created between satellite remote sensing reflectance and in-situ measured TSS concentration. The retrieved results for the whole water area matched the in-situ data well at most stations. The retrieval errors may be related to the problem of scale matching and mixed pixel. In three selected subregions of Poyang Lake, the distribution trend of retrieved TSS was consistent with that of the field investigation. It was shown that HJ-1A/1B CCD imagery can be used to estimate TSS concentrations in Poyang Lake over synoptic scales after applying an appropriate atmospheric correction method and retrieval algorithm.

Keyword: total suspended sediment; HJ-1A/1B CCD; atmospheric correction; retrieval algorithm; Poyang Lake

1 INTRODUCTION

Inland lakes, many of which are closely associated with human activities, now face serious pollution and eutrophication problems. Therefore, it is important to monitor water quality effectively and to understand how the health of freshwater lakes is affected by multifarious natural and anthropogenic factors (Hu et al., 2004). Water is traditionally monitored by taking point samples at regular intervals during field investigations. This traditional way, with only a few discrete stations is not only money- and time-consuming, but also inadequate to observe temporal and spatial variations over a large area. Thus, a monitoring tool is needed that can provide long-term, routine observations of water quality bio-optical indicators.

Remote sensing could be used as a survey tool by water management authorities, allowing the collection

* Supported by the National Basic Research Program of China (973 Program) (No. 2011CB707106), the National Natural Science Foundation of China (Nos. 41071261, 41023001, 41021061, 40906092, 40971193, 41101415), the Opening Foundation of Institute of Remote Sensing and Earth Sciences, Hangzhou Normal University (No. PDKF2010YG06), the Fundamental Research Funds for the Central Universities, the China Postdoctoral Science Foundation (No. 20100480861), LIESMARS Special Research Funding, the Natural Science Foundation of Hubei Province, China (No. 2009CDB107), and the Natural Science Foundation of Zhejiang Province, China (No. Y5090143)
** Corresponding authors: cecxl@yahoo.com; tianye2003@gmail.com

of water quality data over a large area simultaneously (Dekker et al., 2001, 2002). Satellite sensors, such as ocean color sensors like the Coastal Zone Color Scanner (CZCS), the Sea-viewing Wide Field-of-view Sensor (SeaWiFS), the Medium Resolution Imaging Spectrometer (MERIS), and the Moderate Resolution Imaging Spectroradiometer (MODIS); and land-use sensors such as the Landsat series and EO-1 Advanced Land Imager (ALI), each with various spectral and spatial-temporal resolutions, can provide synoptic water quality data (Chen et al., 2004). There have been efforts to estimate water quality using ocean color sensors data (Chen et al., 2009a, 2011; Hu et al., 2004; Wang et al., 2011), and land-use sensors data (Chen et al., 2009b; Hui et al., 2008; Jenson et al., 1989; Lathrop et al., 1990; Oyama et al., 2009; Wang et al., 2004; Wu et al., 2008). Although ocean color sensors have short revisit times with high spectral resolution and sensitivity, the spatial resolution is typically too coarse to describe water quality features adequately (e.g., the highest spatial resolution of MODIS is only 250 m), and the long revisit time of land-use sensors (e.g., the revisit time for Landsat TM is 16 days), makes these data inadequate to monitor water quality variation in dynamic water bodies.

The "environment and disaster monitoring and forecasting small satellite constellations" (HJ-1A/1B satellites), launched by China on September 6, 2008, bring a new water-quality monitoring opportunity. Both the HJ-1A and HJ-1B satellites are equipped with two charge-coupled device (CCD) cameras that are the same in nadir symmetry, design parameters, and characteristics. The CCD cameras capture four spectral bands (430–520 nm, 520–600 nm, 630–690 nm, and 760–900 nm) with a scan swath of 360 km (≥700 km with 2 sensors), recorded data of 8 bits, and a signal-to-noise ratio ≥48 dB; the constellation of the two satellites generates multi-spectrum CCD images with both high spatial resolution (30 m) and short revisit time (2 days) (http://www.cresda.com/n16/n1130/n1582/8384.html). The HJ-1A/1B CCD could be an ideal tool to provide rapid, repeated, and simultaneous synoptic monitoring of inland lake water environment parameters. Total suspended sediment (TSS) concentration is an important water quality indicator of turbidity, riverine flux, bank erosion, and current- or wind-generated resuspension (Hu et al., 2004; Fulweiler and Nixon, 2005). Taking Poyang Lake in Jiangxi Province of China as an example, this paper demonstrates the potential to monitor TSS in inland lakes using HJ-1A/1B CCD.

2 STUDY AREA AND DATA SOURCES

Poyang Lake (28°22′N–29°45′N, 115°47′E–116°45′E), with a maximum inundation area of >3 000 km^2 during the flooding season (Feng et al., 2011), is the largest fresh water lake in China. It is located in northern Jiangxi Province and south of the middle and lower reaches of the Changjiang (Yangtze) River (Fig.1). The lake has five main tributaries (Ganjiang River, Fuhe River, Xinjiang River, Raohe River, and Xiushui River) and flows from south to north to discharge into the Changjiang River through a narrow outlet at Hukou. Annually, the mean temperature around the lake is 16–18°C with a frost-free period of 240–330 d, and the rainfall is 1 340–1 780 mm (Zhang, 1988). The seasonality of precipitation leads to rapid changes in the level of the lake. During the wet season (from April to September), marshlands are inundated, thus increasing the water surface. During the dry season (from October to March of the next year) the water subsides, exposing a mass of grass-covered marshlands and the lake loses as much as 90% of its water. This forms seasonal variations of floods in summer and marshlands in winter in the lake water.

To better study Poyang Lake, three subregions (A, B, C) were selected as the main study areas according to their unique characteristics of water quality conditions (Fig.1). The latitude increases from Subregion C to A. Subregion A is located between Hukou and the north side of Songmen Mountain, where sand dredging is active and the water is highly turbid because of strong resuspension of sediment. Subregion B is located south of Songmen Mountain, near the main water body where the water is moderately turbid; there are many marshlands in the area, so it suffers little influence of anthropogenic activity. Subregion C is close to Raohe River mouth and surrounded by farmland and villages, so it is susceptible to anthropogenic activity and has low-level turbid water.

The field surveys were conducted from October 17–26, 2009 in Poyang Lake, in the dry season. Many marshlands had emerged and the lake had less water. In total, 90 water samples were collected during the surveys; the locations of the sampling stations are shown in Fig.1. At each discrete station, above-water spectral remote sensing reflectance (R_{rs}) was measured with a SVC HR-1024 field portable spectroradiometer (Spectra Vista Corporation, 2009), using methods recommended by Lee et al. (1997)

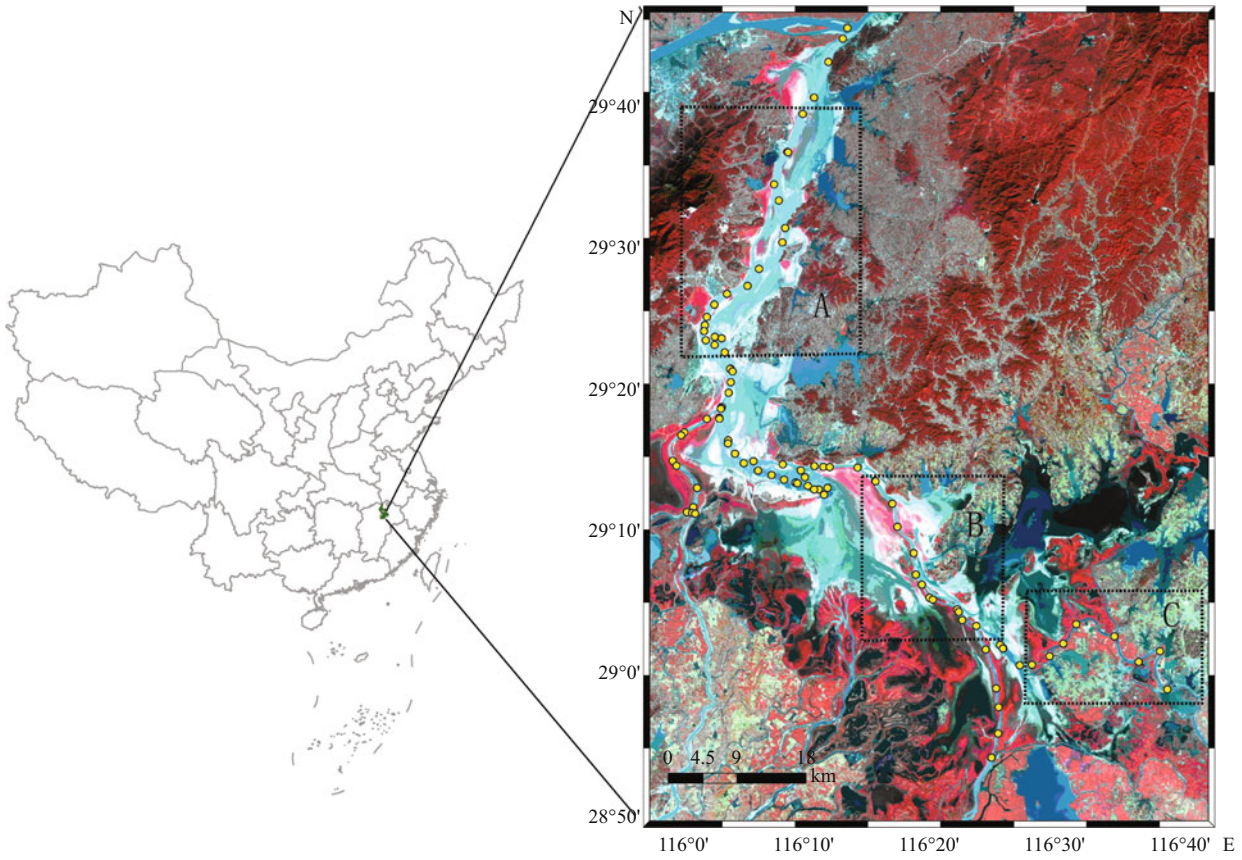

Fig.1 HJ-1A/1B CCD image (Red: 760–900 nm, Green: 630–690 nm, Blue: 520–600 nm) collected on October 24, 2009, showing the study area and location of Poyang Lake in China

Yellow points represent the positions of sampling stations, and black rectangles represent Subregions A, B, and C.

and Mobley (1999). Four reflectance peaks around 580 nm, 650 nm, 700 nm, and 810 nm can be seen in the remote sensing reflectance curves of sampling stations in Poyang Lake (Fig.2). The reflectance peak around 580 nm is due to the decreased absorbance of colored dissolved organic matter (CDOM) and

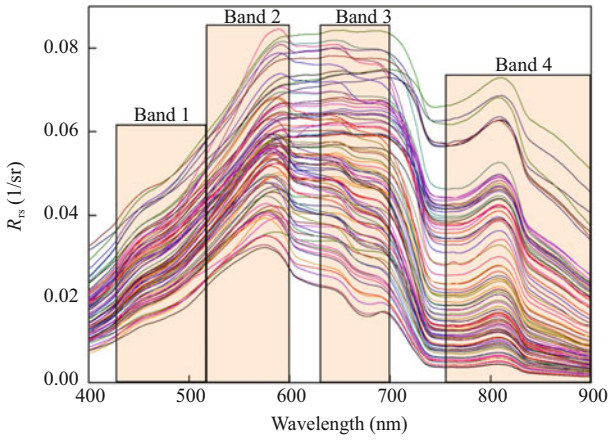

Fig.2 Spectral remote sensing reflectance curves of sampling stations in Poyang Lake, and HJ-1A/1B CCD band ranges

de-pigmented particle before 580 nm and meanwhile the dramatically increased absorbance of pure water after 580 nm The obvious absorbance peaks of phycocyanin around 620 nm and chlorophyll *a* around 675 nm cause the reflectance peak around 650 nm. The reflectance peak around 700 nm is due to the obvious absorbance peak of chlorophyll *a* around 675 nm and the dramatically increased absorbance of pure water after 700 nm. There is one local absorbance vale of pure water around 810 nm leading to the reflectance peak around 810 nm. The atmospheric aerosol optical depth (AOD) was measured by a MICROTOPS II hand-held sun photometer. Surface water samples were collected and analyzed in the laboratory for TSS concentration (TSSC), chlorophyll-*a* concentration, and CDOM absorption coefficient at 400 nm (ag(400)). The 0.45 μm Whatman glass fiber membrane filters were used to extract TSS, while 0.45 μm Whatman acetate fiber membrane filters were used to extract chlorophyll *a*. To measure CDOM absorption, water samples were filtered through 0.2 μm Millipore membrane filters, then the absorbance data were analyzed using an Ocean Optics HR2000 spectrometer,

a PX-2 light source, and a liquid waveguide capillary cell with 1 m optical path length, and finally the absorbance data were converted to an absorption coefficient (Hu et al., 2002). The HJ-1A/1B CCD imagery generated at 11:13 a.m. on October 24, 2009 with a spot of cloud cover was selected to retrieve TSS, while MODIS obtained at 10:20 a.m. on the same day was used to derive the aerosol optical data. On the basis of in-situ data from the field investigation for the subregions (Subregion A, B, and C), the water depth is greater than three times the water transparency in Poyang Lake (Table 1), so the lake bottom effect was ignored (Lodhi and Rundquist, 2001).

3 ATMOSPHERIC CORRECTION

An atmospheric correction method was applied to process the HJ-1A/1B CCD imagery with the aid of Terra/MODIS aerosol information (Tian et al., 2010). HJ-1A/1B CCD and Terra/MODIS are in sun-synchronous orbits, and have descending nodes around 10:30 a.m. local time. Aerosol changes during the time difference (< 1 h) would be very small, and the same cross-sensor approach has been used elsewhere (e.g., Hu et al., 2001, LANDSAT-7/ETM+ versus SeaWiFS; Pan et al., 2003, CMODIS versus SeaWiFS; Pan et al., 2004, HY-1A COCTS versus SeaWiFS; Tang et al., 2005, CEBERS-02 CCD versus MODIS; Wang and Franz, 2000, MOS versus SeaWiFS). The atmospheric aerosol optical depth (AOD) properties of Terra/MODIS, achieved by a simple extension of the near infrared-shortwave infrared (NIR-SWIR) combined atmospheric correction approach embedded in SeaWiFS Data Analysis System (SeaDAS) (Wang and Shi, 2007), can be used to correct the simultaneous HJ-1A/1B CCD imagery. The AOD at 551 nm of 0.297 that has the most frequency of occurrences was retrieved from Terra/MODIS, validated by the in-situ measured AOD data of 0.307, and converted into a visibility of 26.3 km according to Eqs.1,2. Then the Fast Line-of-sight Atmospheric Analysis of Spectral Hypercubes (FLAASH) module in ENVI software was used to do the atmospheric correction for the HJ-1A/1B CCD imagery using the visibility data as inputs to get surface reflectance (Fig.3). Finally, the remote sensing reflectance was obtained from the surface reflectance according to Eq.3 and approximate Eq.4.

$$\beta=\frac{AOD}{\alpha} \quad (1)$$

Table 1 Water depth and the water transparency of the sampling stations in the subregions of Poyang Lake

Subregion	Date	Latitude(°N)	Longitude(°E)	W.T. (m)	W.D. (m)
A	Oct 17, 2009	29.614	116.137	0.1	5.0
	Oct 17, 2009	29.659	116.157	0.1	15.0
	Oct 18, 2009	29.386	116.041	0.2	2.5
	Oct 20, 2009	29.525	116.135	0.1	16.0
	Oct 20, 2009	29.557	116.126	0.1	8.0
	Oct 20, 2009	29.508	116.131	0.2	5.0
	Oct 20, 2009	29.476	116.100	0.2	4.5
	Oct 20, 2009	29.446	116.057	0.2	18.0
	Oct 20, 2009	29.409	116.028	0.1	10.0
	Oct 20, 2009	29.391	116.029	0.2	5.5
	Oct 26, 2009	29.377	116.055	0.2	15.0
	Oct 26, 2009	29.394	116.050	0.2	6.5
	Oct 26, 2009	29.396	116.041	0.2	15.0
	Oct 26, 2009	29.402	116.027	0.1	17.5
	Oct 26, 2009	29.419	116.030	0.1	12.5
	Oct 26, 2009	29.434	116.040	0.1	7.5
	Oct 26, 2009	29.456	116.085	0.1	3.5
B	Oct 21, 2009	29.087	116.337	0.3	2.0
	Oct 21, 2009	29.142	116.311	0.3	2.2
	Oct 21, 2009	29.200	116.282	0.3	4.0
	Oct 21, 2009	29.226	116.259	0.3	1.3
	Oct 22, 2009	29.076	116.370	0.4	2.0
	Oct 22, 2009	29.057	116.396	0.3	3.0
	Oct 23, 2009	29.059	116.530	0.9	3.5
	Oct 24, 2009	29.057	116.395	0.6	3.0
	Oct 24, 2009	29.073	116.372	0.5	2.0
	Oct 24, 2009	29.088	116.336	0.4	3.0
	Oct 24, 2009	29.173	116.289	0.4	3.0
	Oct 24, 2009	29.227	116.258	0.3	1.2
C	Oct 23, 2009	29.021	116.494	0.9	4.0
	Oct 23, 2009	29.045	116.581	0.7	3.5
	Oct 23, 2009	29.015	116.614	0.6	3.5
	Oct 23, 2009	28.983	116.652	0.8	4.5
	Oct 24, 2009	29.036	116.512	0.7	4.0
	Oct 24, 2009	29.011	116.470	0.6	4.0

W.T. = water transparency; W.D. = water depth.

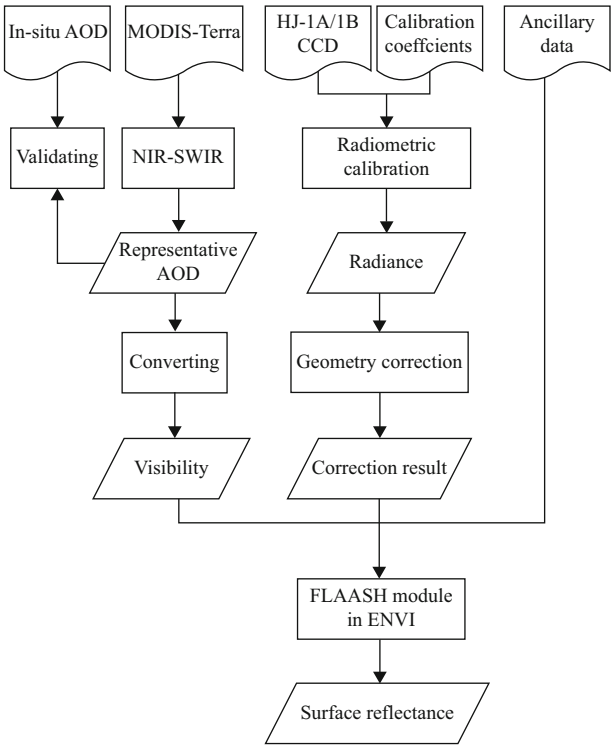

Fig.3 Flow chart for atmospheric correction of the HJ-1A/1B CCD image

$$\upsilon=\frac{3.912}{\beta} \tag{2}$$

where α is the effective aerosol layer thickness, β is the extinction coefficient at 550 nm, and υ is the visibility.

$$R_{\mathrm{rs}}=\rho_{\mathrm{w}}/\pi t_0 \tag{3}$$

$$t_0=\exp(-\tau_{\mathrm{r}}/2/\cos\theta_0) \tag{4}$$

where ρ_{w} is surface reflectance, t_0 is the diffuse transmittance from the sun to the pixel, θ_0 is the solar zenith angle, and τ_{r} is the Rayleigh optical thickness calculated using the method proposed by Hansen and Travis (1974).

The central wavelength of HJ-1A/1B CCD was simulated as (Gordon, 1995):

$$\lambda_{\mathrm{central}}=\frac{\int_{\lambda_1}^{\lambda_2}\mathrm{RSR}(\lambda)\lambda\mathrm{d}\lambda}{\int_{\lambda_1}^{\lambda_2}\mathrm{RSR}(\lambda)\mathrm{d}\lambda} \tag{5}$$

where $\lambda_{\mathrm{central}}$ is the central wavelength, λ is the wavelength and RSR is the relative spectral response function of HJ-1A/1B CCD. The central wavelengths for HJ-1A/1B CCD are 489 nm for band 1, 567 nm for band 2, 664 nm for band 3, and 828 nm for band 4. $R_{\mathrm{rs}}(\lambda_{\mathrm{central}})$ was used to represent the band R_{rs} of HJ-1A/1B CCD

To evaluate the atmospheric correction precision, the in-situ hyperspectral R_{rs} data were integrated over the RSR function of the HJ-1A/1B CCD bands to obtain simulated $R_{\mathrm{rs}}(489)$, $R_{\mathrm{rs}}(567)$, $R_{\mathrm{rs}}(664)$, and $R_{\mathrm{rs}}(828)$ according to the formulas, as:

$$L_{\mathrm{w}}=\frac{\int_{\lambda_1}^{\lambda_2}\mathrm{RSR}(\lambda)L_{\mathrm{w}}(\lambda)\mathrm{d}\lambda}{\int_{\lambda_1}^{\lambda_2}\mathrm{RSR}(\lambda)\mathrm{d}\lambda} \tag{6}$$

$$E_{\mathrm{d}}(0+)=\frac{\int_{\lambda_1}^{\lambda_2}\mathrm{RSR}(\lambda)E_{\mathrm{d}}(\lambda)\mathrm{d}\lambda}{\int_{\lambda_1}^{\lambda_2}\mathrm{RSR}(\lambda)\mathrm{d}\lambda} \tag{7}$$

$$R_{\mathrm{rs}}=\frac{L_{\mathrm{w}}}{E_{\mathrm{d}}(0+)} \tag{8}$$

where λ is wavelength, L_{w} is water-leaving radiance, and $E_{\mathrm{d}}(0+)$ is downwelling irradiance just above the water surface.

Figure 4 shows a comparison between in-situ R_{rs} and satellite R_{rs} of HJ-1A/1B CCD after atmospheric correction at the sampling stations in Poyang Lake. The values of satellite $R_{\mathrm{rs}}(567)$ and $R_{\mathrm{rs}}(664)$ match closely to those of in-situ R_{rs}, but not those of $R_{\mathrm{rs}}(489)$ and $R_{\mathrm{rs}}(828)$. The mean relative difference for satellite $R_{\mathrm{rs}}(567)$ is 11.3% and for $R_{\mathrm{rs}}(664)$ is 15.2%, while the mean relative difference for satellite $R_{\mathrm{rs}}(489)$ is 50.4% and for $R_{\mathrm{rs}}(828)$ is 113.4%. The atmosphere correction method used here worked well at band 2 and band 3, but poorly at band 1 and band 4. This may be related to the factor that the calibration of CCD bands may be off and this may affect band 1 and band 4 more than band 2 and band 3.

4 RETRIEVAL ALGORITHM ESTABLISHMENT

The satellite R_{rs} of HJ-1A/1B CCD bands was extracted for the sampling stations after atmospheric correction. Two thirds of the in-situ TSSC was used to establish the retrieval model and the other one third for the validation. On the basis of the reasonable results of atmospheric correction for band 2 and band 3, the optimal exponential algorithm producing the highest determination coefficient through regression analysis among different band combinations forms for TSSC retrieval was established as:

$$\mathrm{TSSC}=0.4023\mathrm{e}^{(46.457X)},$$
$$X=(R_{\mathrm{rs}}(567)+R_{\mathrm{rs}}(664))R_{\mathrm{rs}}(664)/R_{\mathrm{rs}}(567) \tag{9}$$

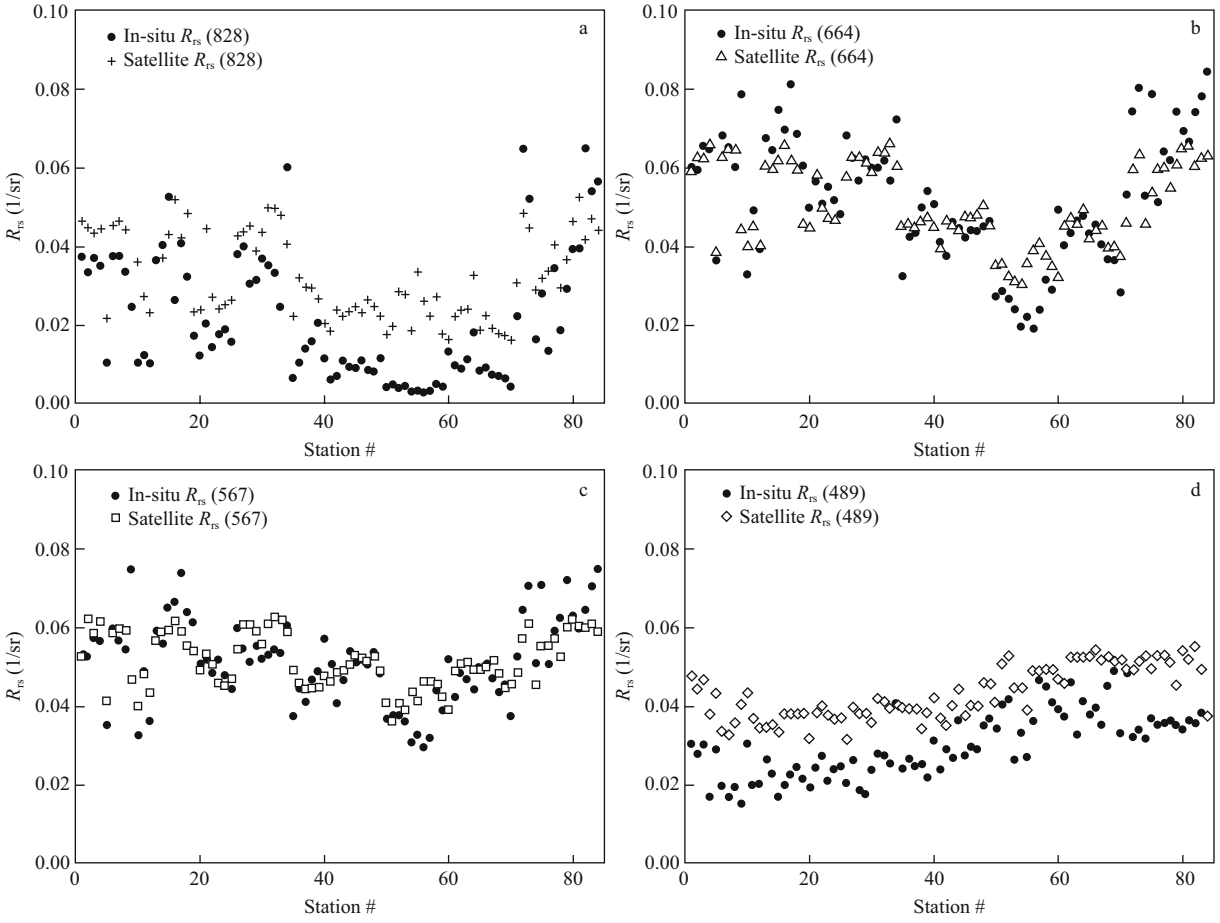

Fig.4 Comparing in-situ data and HJ-1A/1B CCD data in four bands for $R_{rs}(\lambda)$ (1/sr) from the sampling stations in Poyang Lake, after atmospheric correction

where X is the combination factor of R_{rs} at band 2 and band 3 obtained from HJ-1A/1B CCD. The R^2 of the regression relationship is 0.8 (Fig.5), and it is significant below the 0.01 level by F-test. The mean relative error is 25.1% through in-situ data validation. The precision of this algorithm can meet the retrieval demand.

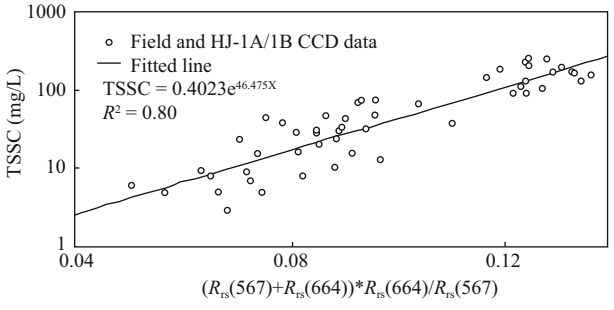

Fig.5 Scatter plot and regression relationship between TSSC and the combination factor of X consisting of R_{rs} at band 2 and band 3 of HJ-1A/1B CCD

5 RESULT AND DISCUSSION

5.1 In-situ water quality indicators

Table 2 shows descriptive statistics including the minimum, maximum, mean, and standard deviation values for the three water quality indicator concentrations of Poyang Lake, according to field measurements taken during the study period, October 17–26, 2009. The variation of TSS in Poyang Lake shows a wide range (3–524 mg/L), while surface chlorophyll-*a* concentration shows a narrow range (0.649–18.582 μg/L) and at the same time the CDOM

Table 2 In-situ water quality indicator concentrations in Poyang Lake from October 17–26, 2009 (S.D.= Standard deviation)

Water quality indicator	Min	Max	Mean	S.D.
TSS (mg/L)	3.0	524.0	85.8	93.982
Chl *a* (μg/L)	0.649	18.582	5.291	3.264
ag(400) (1/m)	0.495	1.170	0.814	0.136

absorption coefficient at 400 ㎚ ranges between 0.495/m and 1.170/m. These numbers demonstrate that the optical characteristics of Poyang Lake water are mainly affected by TSS.

The graph in Fig.6 shows the in-situ TSS of the sampling stations from October 17–26, 2009. To visualize the variation in TSS from south to north, Fig.6 was drawn over latitude from the extreme south sampling site in Poyang Lake to the extreme north sampling site lying at the intersection of Poyang Lake and Changjiang River. Except for the extreme north sampling site with a low TSSC, as latitude increases, the TSSC first starts low and remains approximately unchanged from about 28.90°–29.03°N, then increases with relatively low values in the middle from 29.03°–29.26°N, and finally increases to relatively large values at the end from 29.26°–29.75°N. In general, TSSC increases from south to north. It is partly due to the sand dredging activities which can make strong resuspension of suspended sediment, since there are little sand dredging activities in the south, while there are many ones in the north.

Table 3 shows the descriptive mean and standard deviation values for TSS, chlorophyll *a*, and ag(400) of the three subregions. High TSSC is found in Subregion A, partly due to sand dredging activities. In Subregion C, both chlorophyll *a* and ag(400) show high values, because Subregion C is surrounded by farmland and villages and is easily influenced by runoff from the land. Subregion B suffers little influence of anthropogenic activity and has low concentration of chl *a*. There are fewer sand dredging activities in Subregion B and C compared with Subregion A, and these two subregions show lower TSSC.

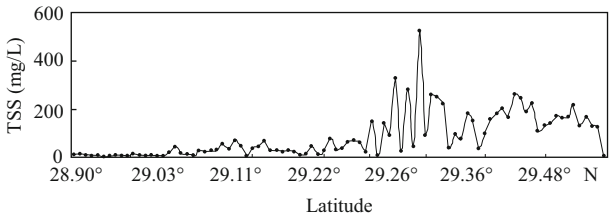

Fig.6 In-situ TSSC from 90 sampling stations from October 17–26, 2009

Table 3 Mean values of TSS, chl *a*, and ag(400) for subregions

Subregion	Mean value/S.D.		
	TSS (mg/L)	Chl *a* (μg/L)	ag(400) (1/m)
A	166.53/53.73	5.84/2.94	0.70/0.05
B	39.77/17.76	4.32/2.35	0.85/0.10
C	6.00/1.60	6.51/3.01	0.83/0.14

S.D.=Standard deviation

5.2 Retrieved results for Poyang Lake as a whole

Using atmospheric correction results and the retrieval algorithm, the TSS distribution was retrieved from a HJ-1A/1B CCD image acquired on October 24, 2009 (Fig.7). The relative errors between the in-situ data and retrieved results for the sampling stations vary because of geography. To analyze the distribution of the differences at different stations, the TSSC retrieved from the HJ-1A/1B CCD image was compared with in-situ TSSC from October 17–26, 2009 (Fig.8). The retrieved TSSC matches closely to the in-situ data at the most southern stations, but diverges sharply at a few middle and northern stations. The high scatter in the in-situ data of Fig.8 also illustrates the high spatial variability of TSS in Poyang Lake. Further, to analyze the concrete

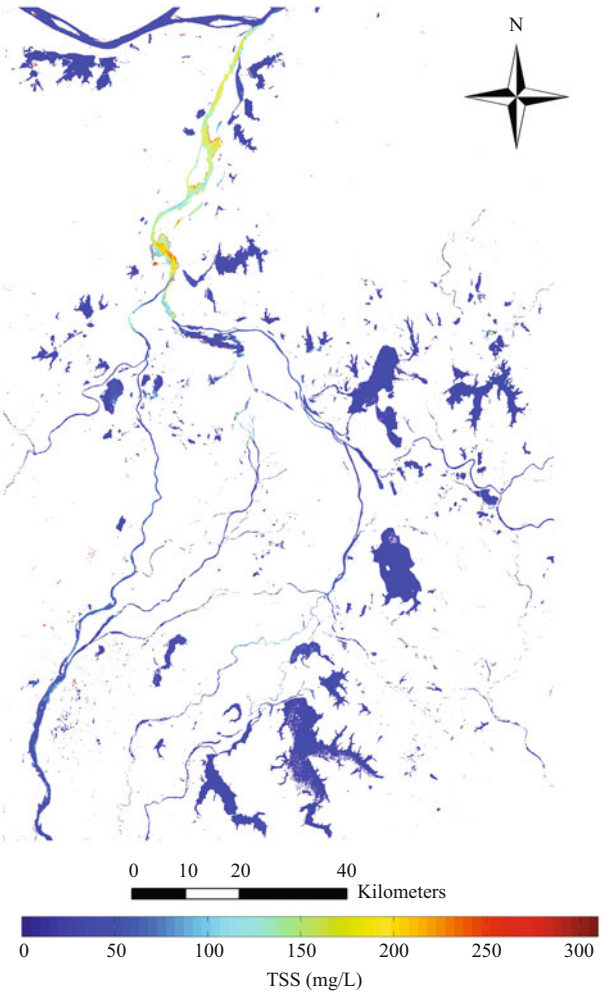

Fig.7 TSS distribution retrieved from HJ-1A/1B CCD image on October 24, 2009

reason for the different retrieval error, two typical sampling stations of October 24, 2009, located at the stream with different width, S102401 and S102402, used to validate the established retrieval model, were chosen for analysis. The absolute error for one sampling station is 0 mg/L and it was 33 mg/L for the other. The error may be related to scale matching and mixed pixel resolutions: first, the in-situ data are from just one point, while the retrieved results are planar data covering a 30 by 30 square meters area, thus generating error; second, the stream width is 900 m, covering 30 pixels at station S102401, while at station S102402, the stream width is just 150 m covering only 5 pixels (Fig.9). Consequently, there is a bigger retrieval difference for station S102402 than for station S102401. Because the land signal influence was more severe for station S102402 than for station S102401, more error was introduced as a result of the mixed pixel problem.

5.3 Retrieved results for subregions of Poyang Lake

From the retrieved TSS results for October 24, 2009, we can see that Subregion A in the sand dredging area had the highest TSSC, Subregion C near the villages and farmland had the lowest TSSC, and Subregion B in the marshlands had TSSC in the middle range (Fig.10). This distribution trend is the same as that found from the in-situ data analysis. Every year, a large amount of sand flows into Subregion A, mainly from the Ganjiang River and the Xiushui River. Driven by big profits, there are many sand dredging activities in Subregion A, and these are the principal factor contributing to strong resuspension of sediment and higher TSSC levels than in subregions B and C. The mean TSSC from the retrieved data is a little lower than the mean in-situ TSSC (Fig.11). This may be related to the uncertainty in atmospheric correction and the established retrieval model.

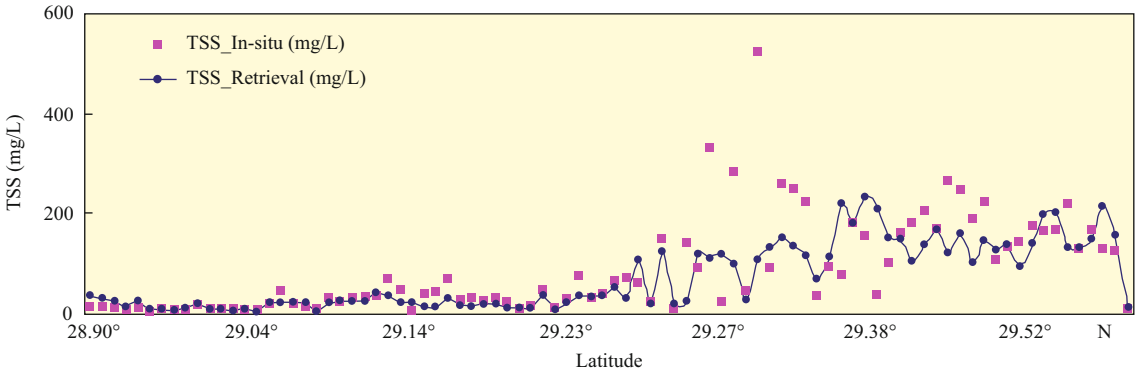

Fig.8 Comparison of TSS concentration between the retrieval values from the HJ-1A/1B CCD image of October 24, 2009 and the in-situ data of October 17–26, 2009

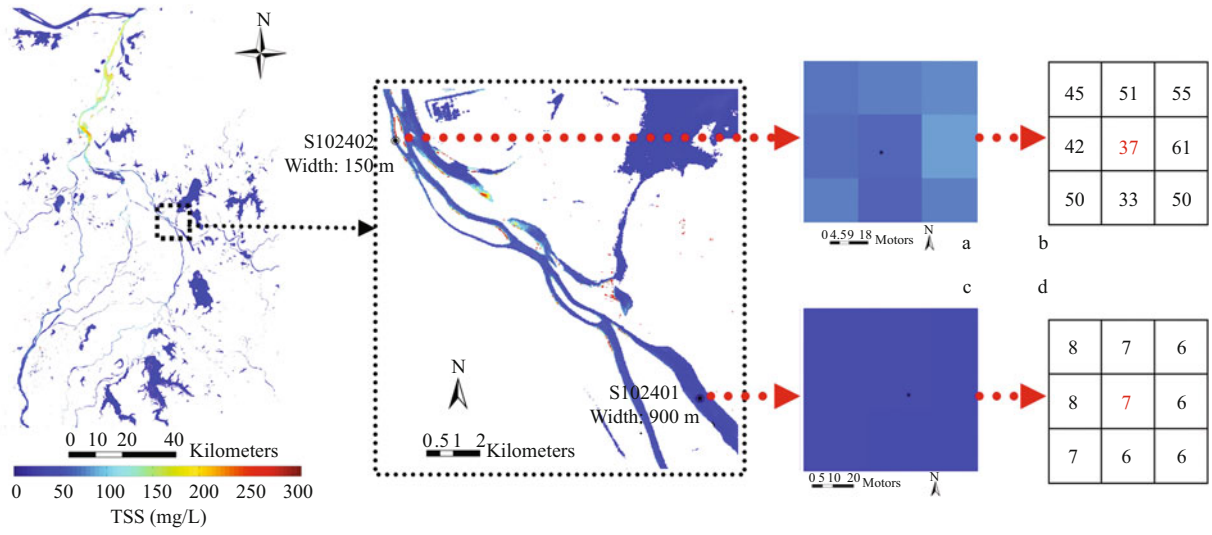

Fig.9 Location of and retrieval values around the two typical sampling stations on October 24, 2009

a. enlarged nine pixels around S102402; b. pixel values around S102402; c. enlarged nine pixels around S102401; d. pixel values around S102401.

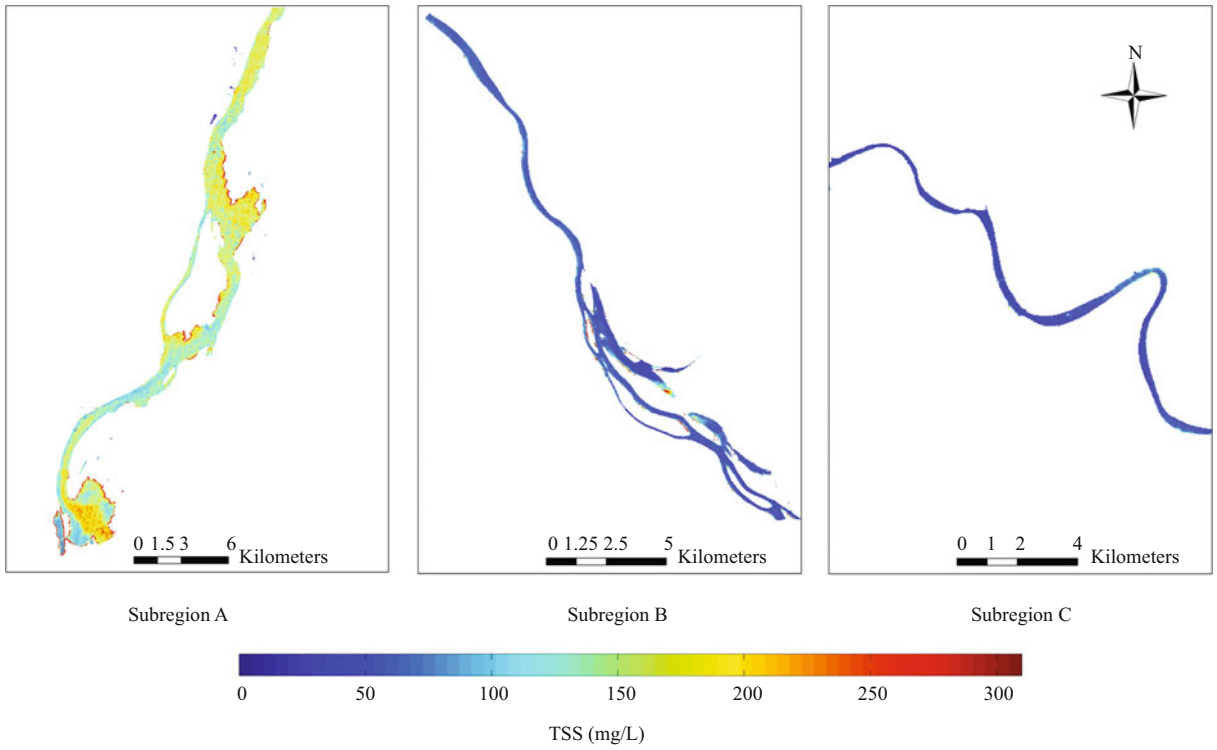

Fig.10 Enlarged maps of TSS distribution for Subregions A, B and C (see Fig.1) over Poyang Lake on October 24, 2009

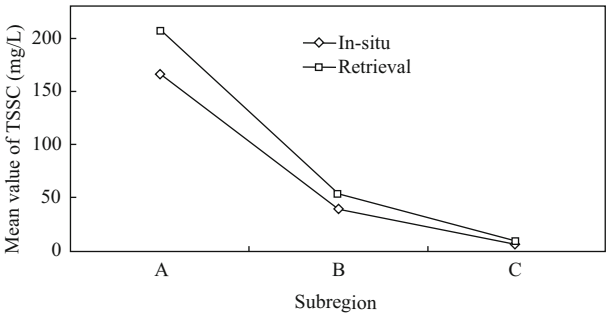

Fig.11 Comparing mean values of TSSC (mg/L) between in-situ measurements and HJ-1A/1B CCD retrieval values for Subregions A, B, and C

6 CONCLUSION AND FUTURE WORK

We conducted field surveys in Poyang Lake to measure water quality parameters (TSSC, chlorophyll-*a* concentration, and CDOM absorption coefficient) and remote sensing reflectance from October 17–26, 2009. The objectives were to study characteristics of Poyang Lake in the dry period, and to evaluate if and how HJ-1A/1B CCD data can be used for inland lake TSS monitoring.

The atmospheric correction for HJ-1A/1B CCD imagery was done using the FLAASH module in ENVI with the aid of aerosol information retrieved from concurrent Terra/MODIS data with a simple extension of the NIR-SWIR combined atmospheric correction approach. Compared with simulated in-situ R_{rs} for the HJ-1A/1B CCD bands, the mean relative difference for atmospheric correction is smaller in the bands with relatively high reflectance, but larger in the bands with low reflectance.

The TSSC distribution in Poyang Lake was retrieved from HJ-1A/1B CCD data on October 24, 2009 using the atmospheric correction results and established retrieval model. The retrieval error may be related to scale matching and mixed pixel resolution. The distribution trend of TSS for the subregions was consistent with the field investigation results. It was shown that the HJ-1A/1B CCD cameras have the potential to monitor TSS in Poyang Lake after applying the proper atmospheric correction method and retrieval model.

In future work, the retrieval of chlorophyll-*a* concentration and CDOM absorption coefficient will be studied, even though this will be difficult because of the limitations of spectral resolution and sensitivity of HJ-1A/1B CCD. Further work will also focus on the improvement of atmospheric correction of HJ-1A/1B CCD in the bands with relatively low remote sensing reflectance so as to better use HJ-1A/1B CCD data in water environmental monitoring and management.

References

Chen X, Li Y S, Liu Z, Yin K, Li Z, Wai O W, King B. 2004. Integration of multi-source data for water quality classification in the Pearl River estuary and its adjacent coastal waters of Hong Kong. *Continental Shelf Research*, **24** (16): 1 827-1 843.

Chen S, Huang W, Wang H, Li D. 2009a. Remote sensing assessment of sediment re-suspension during Hurricane Frances in Apalachicola Bay, USA. *Remote Sensing of Environment*, **113**(12): 2 670-2 681.

Chen S, Fang L, Zhang L, Huang W. 2009b. Remote sensing of turbidity in seawater intrusion reaches of Pearl River Estuary–a case study in Modaomen water way, China. *Estuarine*, *Coastal and Shelf Science*, **82**(1): 119-127.

Chen S, Huang W, Chen W, Wang H. 2011. Remote sensing analysis of rainstorm effects on sediment concentrations in Apalachicola Bay, USA. *Ecological Informatics*, **6**(2): 147-155.

Dekker A G, Vos R J, Peters S W M. 2001. Comparison of remote sensing data, model results and in-situ data for total suspended matter (TSM) in the southern Frisian lakes. *The Science of the Total Environment*, **268**: 197-214.

Dekker A G, Vos R J, Peters S W M. 2002. Analytical algorithms for lake water TSM estimation for retrospective analysis of TM and SPOT sensor data. *International Journal of Remote Sensing*, **23**(1): 15-35.

Feng L, Hu C, Chen X, Li R, Tian L, Murch B. 2011. MODIS observations of the bottom topography and its inter-annual variability of Poyang Lake. *Remote Sensing of Environment*, **115**(10): 2 729-2 741.

Fulweiler R, Nixon S. 2005. Export of nitrogen, phosphorus, and suspended solids from a southern New England watershed to Little Narragansett Bay. *Biogeochemistry*, **76**: 567-593.

Gordon H R. 1995. Remote sensing of ocean color: a methodology for dealing with broad spectral bands and significant out-of-band response. *Applied Optics*, **34**(36): 8 363-8 374.

Hansen J E, Travis L D. 1974. Light scattering in planetary atmospheres. *Space Science Reviews*, **16**: 527-610.

Hu C, Chen Z, Clayton T D, Swarzenski P, Brock J C, Muller-karger F E. 2004. Assessment of estuarine water-quality indicators using MODIS medium-resolution bands: Initial results from Tampa Bay, Florida. *Remote Sensing of Environment*, **93**: 423-441.

Hu C, Muller-Karger F E, Andrefouet S, Carder K L. 2001. Atmospheric correction and cross-calibration of LANDSAT-7/ETM+ imagery over aquatic environments: A multiplatform approach using SeaWiFS/MODIS. *Remote Sensing of Environment*, **78**: 99-107.

Hu C, Muller-Karger F E, Zepp R G. 2002. Absorbance, absorption coefficient, and apparent quantum yield: a comment on common ambiguity in the use of these optical concepts. *Limnology and Oceanography*, **47**: 1 261-1 267.

Hui F, Xu B, Huang H, Yu Q, Gong P. 2008. Modeling spatial-temporal change of Poyang Lake using multi-temporal Landsat imagery. *International Journal of Remote Sensing*, **29**(20): 5 767-5 784.

Jenson J R, Kjerfve B, Ramsey III E W et al. 1989. Remote sensing and numerical modeling of suspended sediment in Laguna de terminos, Campeche, Mexico. *Remote Sensing of Environment*, **28**: 33-44.

Lathrop R G, Vande Castle J R, Lillesand T M. 1990. Monitoring river plume transport and mesoscale circulation in Green Bay, Lake Michigan, through satellite remote sensing. *Journal of Great Lakes Research*, **16**(3): 471-484.

Lee Z, Carder K L, Steward R G, Peacock T G, Davis C O, Mueller J L. 1997. Remote-sensing reflectance and inherent optical properties of oceanic waters derived from above-water measurements. *Ocean Optics*, *XIII*, SPIE **2963**: 1 960-1 966.

Lodhi M A, Rundquist D C. 2001. A spectral analysis of bottom-induced variation in the colour of Sand Hills lakes, Nebraska, USA. *International Journal of Remote Sensing*, **22**: 1 665-1 682.

Mobley C D. 1999. Estimation of the remote sensing reflectance from above-surface measurements. *Applied Optics*, **38**: 7 442-7 455.

Oyama Y, Matsushita B, Fukushima T, Matsushige, Imai A. 2009. Application of spectral decomposition algorithm for mapping water quality in a turbid lake (Lake Kasumigaura, Japan) from Landsat TM data. *ISPRS Journal of Photogrammetry and Remote Sensing*, **64**(1): 73-85.

Pan D, He X, Mao T. 2003. Preliminary study on the orbit cross-calibration of CMODIS by seawifs. *Progress in natural Science*, **13**(10): 745-749.

Pan D, He X, Zhu Q. 2004. In-orbit cross-calibration of HY-1A satellite sensor COCTS. *Chinese Science Bulletin*, **49**: 2 521-2 526.

Spectra Vista Corporation. 2009. HR-1024/HR-768 User Manual, Revision 1.8. Spectra Vista Corporation, New York, USA. 125p.

Tang J, Gu X, Niu S, Ma C, Min X. 2005. Water target based cross-calibration of CEBERS-02 CCD camera with MODIS data. *Science in China Ser*. *E Engineering and Materials Science*, **48** (Supp I): 61-71.

Tian L, Lu J, Chen X, Yu Z, Xiao J, Qiu F, Zhao X. 2010. Atmospheric correction of HJ-1A/1B CCD images over Chinese coastal waters using Terra/MODIS aerosol data. *Science China*: *Technological Sciences*, **53**: 191-195.

Wang M, Franz BA. 2000. Comparing the ocean color measurements between MOS and SeaWiFS: a vicarious intercalibration approach for MOS. *IEEE Transactions on Geoscience and Remote Sensing*, **38**: 184-187.

Wang M, Shi W. 2007. The NIR-SWIR combined atmospheric correction approach for MODIS ocean color data processing. *Optics Express*, **15**(24): 15 722-15 733.

Wang M, Shi W, Tang J. 2011. Water property monitoring and assessment for China's inland Lake Taihu from MODIS-Aqua measurements. *Remote Sensing of Environment*, **115**(3): 841-854.

Wang Y, Xia H, Fu J, Sheng G. 2004. Water quality change in reservoirs of Shenzhen, China: detection using LANDSAT/TM data. *Science of the Total Environment*, **328**: 195-206.

Wu G F, De L J, Skidmore A K, Prins Herbert H T, Liu Y. 2008. Comparison of MODIS and Landsat TM5 images for mapping tempo-spatial dynamics of Secchi disk depths in Poyang Lake national nature reserve, China. *International Journal of Remote Sensing*, **29**(8): 2 183-2 198.

Zhang B. 1988. Study on Poyang Lake. Shanghai Publishing House of Science and Technology, Shanghai, China. p.3-143. (in Chinese)